ESD-TR-88-312

Technical Report
823

Optical Spatial Tracking Using Coherent Detection in the Pupil Plane

E.A. Swanson
G.M. Carter
D.J. Bernays
D.M. Hodsdon

19 May 1989

Lincoln Laboratory
MASSACHUSETTS INSTITUTE OF TECHNOLOGY
LEXINGTON, MASSACHUSETTS

Prepared for the Department of the Air Force
under Electronic Systems Division Contract F19628-85-C-0002.

The work reported in this document was performed at Lincoln Laboratory, a center for research operated by Massachusetts Institute of Technology, with the support of the Department of the Air Force under Contract F19628-85-C-0002.

This technical report has been reviewed and is approved for publication.

FOR THE COMMANDER

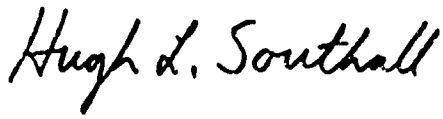

Hugh L. Southall, Lt. Col., USAF
Chief, ESD Lincoln Laboratory Project Office

MASSACHUSETTS INSTITUTE OF TECHNOLOGY
LINCOLN LABORATORY

OPTICAL SPATIAL TRACKING USING COHERENT DETECTION IN THE PUPIL PLANE

E.A. SWANSON
G.M. CARTER
D.J. BERNAYS
Group 67

D.M. HODSDON
Group 63

TECHNICAL REPORT 823

19 MAY 1989

ABSTRACT

Design considerations for a heterodyne spatial tracking system utilizing pupil-plane processing techniques and its advantages over traditional focal-plane processing are described. Noise performance bounds, optimal and suboptimal local oscillator distributions, pull-in performance, and applications other than spatial tracking are discussed. Experimental verification of a one-axis closed-loop tracking system is presented.

TABLE OF CONTENTS

LIST OF ILLUSTRATIONS

ACKNOWLEDGMENTS

We would like to acknowledge the valuable contributions received from Roy Bondurant, Don Boroson, Vincent Chan, Ed Bucher, Linden Mercer, Doug Marquis, and John Kaufmann. Thanks are also due to Joseph Miazga for assembling and aligning the optical layout used in this experiment.

OPTICAL SPATIAL TRACKING USING COHERENT DETECTION IN THE PUPIL PLANE

1. INTRODUCTION

Almost all radar and communications systems require stabilization to a fraction of an antenna beamwidth. At optical frequencies, where antenna beamwidths can be extremely narrow (~ μradians), spatial tracking issues play a dominant role in system design and performance. Spatial tracking systems based on coherent (heterodyne, homodyne) or noncoherent (direct) detection can be used. Although direct detection systems are the most commonly used and analyzed, coherent detection is the preferred choice in many instances. Such instances arise when increased sensitivity is needed, especially in the presence of background, or in coherent radar and communication systems where it is natural to integrate a coherent tracker and a coherent receiver.

Spatial tracking systems which employ coherent detection have been the subject of many studies [1-6]. These studies have focused on optical detection in the focal-plane, i.e., focal-plane processing. In the focal plane there is a linear relationship between focal spot lateral displacement and incidence angle (see Figure 1). A tracking error sensor can be formed by placing a quadrant detector in the focal plane and processing the outputs to extract the tracking information that is contained in the relative amplitudes of the four detector outputs. Alternatively optical detection may be performed in the pupil plane [see Figures 2(a) and 2(b)]. In this case a tracking sensor can be formed by placing a quadrant detector in the pupil plane and processing the outputs. However, in pupil-plane processing the tracking information is contained in the relative phases of the four detector outputs. Note that although focal-plane processing techniques are applicable to both heterodyne and direct detection, pupil-plane processing is only possible with coherent detection schemes.

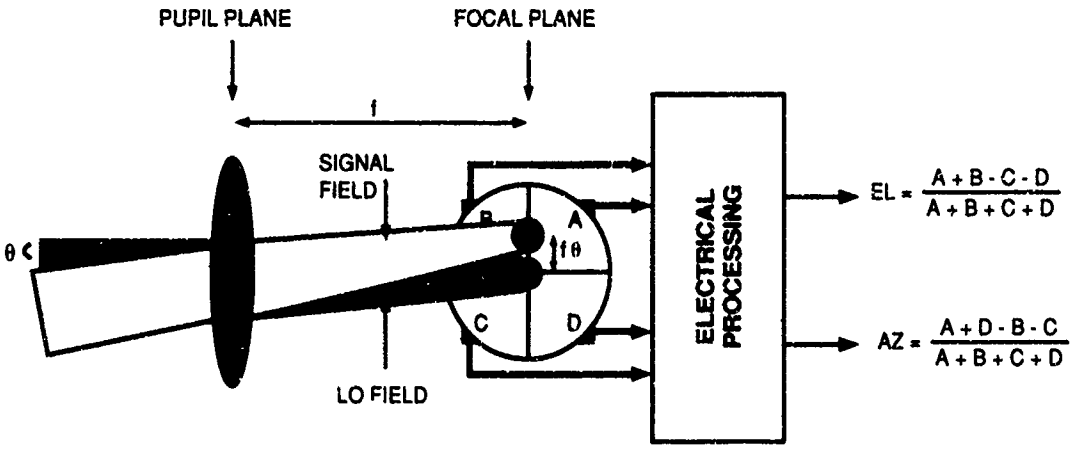

Figure 1. Focal-plane processing.

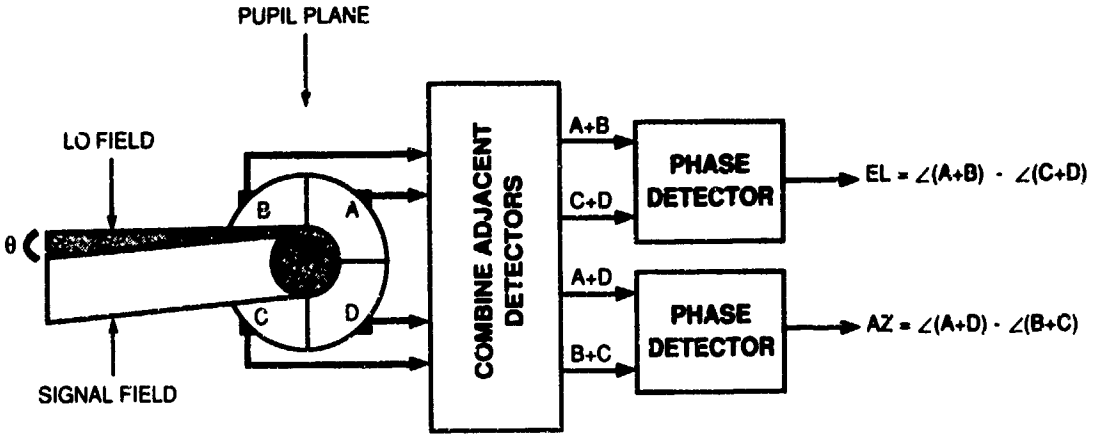

Figure 2(a). Pupil-plane processing (phase processing).

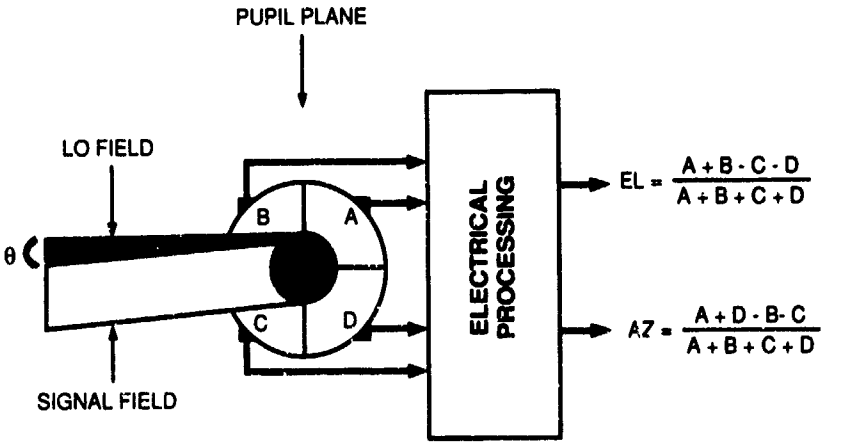

Figure 2(b). Pupil-plane processing (amplitude processing).

It is possible to show that for arbitrary detector arrays and electrical processing there is no theoretical advantage, in the linear region of the angle discriminator or otherwise, by either processing technique. That is because coherent detection and all passive optical systems are invertible linear transformations. Equivalently, there is no information lost as the signal field propagates from the pupil plane to the focal plane. However, when implementation issues (such as receiver complexity) are considered, a number of attractive features of pupil-plane processing become apparent. For instance, in order to overcome the power loss and discriminator distortions that result from the dead-zone (between 1 to 5 μm in size for a good device) associated with focal-plane quadrant detectors or image-splitters one must use long focal length lenses (large f numbers) or complex telephoto lenses (see Figure 3). The resultant system is usually large and alignment-sensitive. Pupil-plane systems are far less sensitive to this loss since in most cases the pupil size is naturally larger than the dead zone and since pupil-plane dead zones will not distort the discriminator. As another example, high-bandwidth quadrant detectors with narrow dead zone and low cross talk for focal-plane systems are difficult to obtain, which usually results in systems which employ large, bulky, alignment-sensitive image-splitting techniques. Although these same techniques can also be used in the pupil plane, an alternative is to use four discrete detectors and a four-element lens to obtain a compact high performance detector. As seen in Figure 4, the dead zone and cross talk between detectors is not a concern, and the dead zone within the focusing lens can easily be made small compared to the signal field diameter.

The following sections will discuss pupil-plane processing issues in more depth. The next section will present unbiased Cramér-Rao bounds on the noise performance of a pupil-plane tracking system and compare them with the focal plane. Section 3 will investigate suboptimal local oscillator distributions and compare their performance with the optimal distribution. In Section 4, a comparison of pull-in performance of focal plane and pupil-plane tracking systems will be inferred from their off-axis discriminator characteristics. Section 5 will briefly investigate some potential applications of pupil-plane processing using higher order arrays. Experimental results for a one-axis closed-loop tracking system are presented in Section 6.

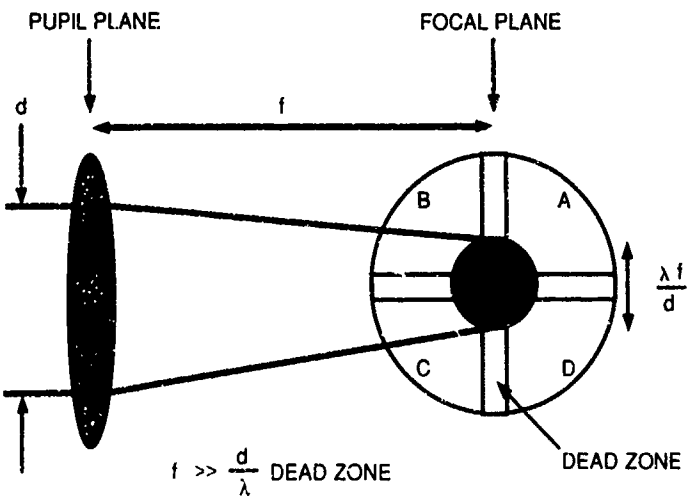

111375-4

Figure 3. Dead zone consideration

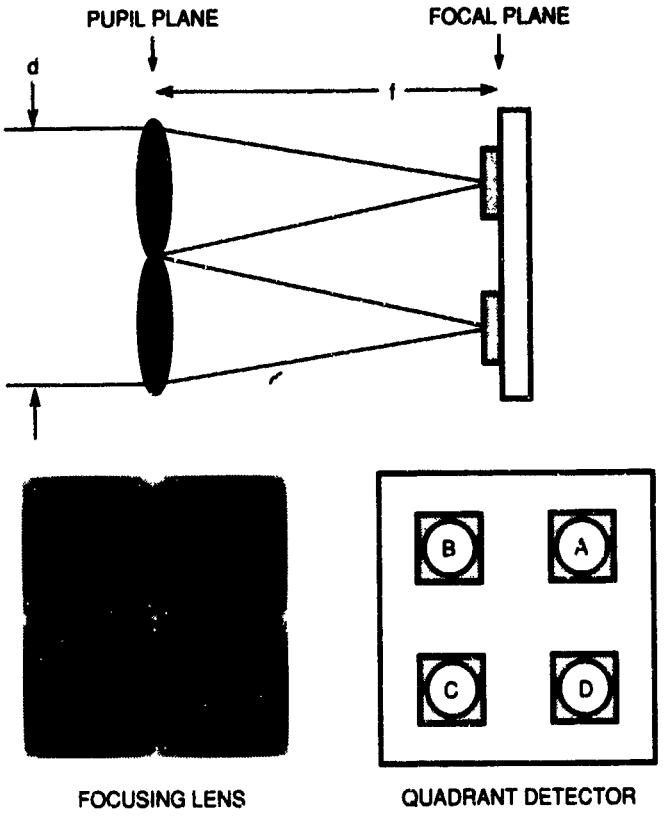

111375-5

Figure 4. Pupil-plane tracking sensor

2. PERFORMANCE BOUNDS

In this section we develop bounds on the noise equivalent angle (NEA) of a heterodyne spatial tracking system operating in the pupil plane. A pupil plane can be considered a perfect image of the entrance aperture of an optical telescope, or alternatively, a plane in which the power distribution is constant with angle. Let the signal and local oscillator fields in the pupil plane be represented by

$$\mathbf{S} = \sqrt{P_s}\; S(x,y)\, e^{-jk(x\theta_x + y\theta_y)}\, e^{-j\omega t} \tag{1}$$

$$\mathbf{L} = \sqrt{P_l}\; L(x,y)\, e^{-j(\omega + \Delta\omega)t} \tag{2}$$

where **S** is the signal field distribution, **L** is the local oscillator field distribution, P_s is the power in the signal field, P_l is the power in the local oscillator field, $k = (2\pi/\lambda)$ is the wave number, λ is the wavelength $\omega = (2\pi f)$ is the optical frequency, $\Delta\omega$ is the I F frequency, t is time, x and y are the two spatial parameters, and θ_x and θ_y are the two angular tracking errors (assumed small). S(x,y) and L(x,y) are the complex amplitudes of the signal and local oscillator fields, respectively. **S** and **L** are assumed to be nominally propagating in the **z** direction. They have been normalized so that

$$1 = \int_{-\infty}^{\infty} |S(x,y)|^2\, dx\, dy = \int_{-\infty}^{\infty} |L(x,y)|^2\, dx\, dy \tag{3}$$

For simplicity we assume that S(x,y) and L(x,y) are symmetric about the x and y axes. Further, we will assume that the detector array is an infinite area quadrant detector. Note that the performance bounds are valid for a detector array with an infinite number of detector elements since L(x,y) can be arbitrarily shaped and we assume linear processing. That is, a given method of linear post detection processing (multiplying, adding, and subtracting) on an infinite detector array can also be done with an infinite area quadrant detector and the proper shaping of the local oscillator field distribution (magnitude and phase).

If the sum is generated by the sum of all four quadrants and the azimuth angular error signal is generated by the sum of the right two quadrants minus the sum of the left two quadrants, then

$$\text{Sum} = \sqrt{2P_s}\; m(\theta_x,\theta_y)\cos(\Delta\omega t) + w_{\text{Sum}}(t) \tag{4}$$

$$\text{Az} = \sqrt{2P_s}\; K_{\text{Az}}(\theta_x,\theta_y)\; \theta_x \sin(\Delta\omega t) + w_{\text{Az}}(t) \tag{5}$$

where

$$m(\theta_x,\theta_y) = \frac{2\int_0^\infty\int_0^\infty S(x,y)\, L(x.y)\cos(kx\theta_x)\cos(ky\theta_y)\,dx\,dy}{\sqrt{\int_0^\infty\int_0^\infty |L(x,y)|^2\,dx\,dy}} \tag{6}$$

$$K_{Az}(\theta_x,\theta_y) = \frac{2\int_0^\infty\int_0^\infty S(x,y)\, L(x,y)\,\mathrm{sinc}(kx\theta_x/\pi)\cos(ky\theta_y)\,dx\,dy}{\sqrt{\int_0^\infty\int_0^\infty |L(x,y)|^2\,dx\,dy}} \tag{7}$$

and $w_{Sum}(t)$ and $w_{Az}(t)$ are the spectrally white Gaussian noise in the sum and difference channel, respectively. The double-sided spectral height of the noise is equal to $h\nu/(2\eta)$, where h is Planck's constant, ν is the optical frequency, and η is the quantum efficiency. The magnitude squared of $m(\theta)$ is often referred to as the sum channel mode-matching efficiency. By analogy, the magnitude squared of $K_{Az}(\theta)$ could be referred to as the azimuth channel mode-matching efficiency. However, it is more commonly known as the azimuth channel discriminator gain.

By taking advantage of the symmetry of the sum and difference channels, an equation describing the normalized signal out of the right two quadrants can be derived.[1] This equation after normalization to the same noise spectral density as above, which illustrates the dependence of the phase of the I F signal on tracking error, is given by

$$Az_+ = \sqrt{2P_s}\sqrt{\frac{m(\theta_x,\theta_y)^2 + (K_{Az}(\theta_x,\theta_y)\theta_x)^2}{2}} \cos\left(\Delta\omega t - \tan^{-1}\left[\frac{K_{Az}(\theta_x,\theta_y)\theta_x}{m(\theta_x,\theta_y)}\right]\right) + w_{Az_+}(t) \tag{8}$$

[1] This is given by $Az_+ = (Sum + Az)/\sqrt{2}$.

For small tracking errors (i.e., $|\theta| < \lambda/d$) the trigonometric functions can be linearized and Az is linear in θ_x.[2] In order to circumvent the dependence of NEA on tracking loop bandwidth, we will focus on the (single-sided) noise equivalent spectral density (NESD). The quantities are related by

$$NESD = \frac{NEA^2}{NEB} \tag{9}$$

where NEB is the single-sided noise equivalent bandwidth of the closed-loop tracking system. It is easy to show that the NESD is equal to

$$NESD = \left[\frac{\eta P_s}{h\nu} K_{Az}(0)^2\right]^{-1} \tag{10}$$

$$NESD = \left[\frac{\eta P_s}{h\nu} \frac{4\left(\int_0^\infty\int_0^\infty S(x,y)\, L(x,y)\, kx\, dx\, dy\right)^2}{\int_0^\infty\int_0^\infty |L(x,y)|^2\, dx\, dy}\right]^{-1} . \tag{11}$$

From the Schwartz inequality the optimal local oscillator field distribution and minimum single-axis NESD are equal to

$$L(x,y)_{opt} = \kappa S(x,y) \tag{12}$$

$$NESD_{opt} = \left[\frac{\eta P_s}{h\nu} \int_{-\infty}^{\infty}\int_{-\infty}^{\infty} |kxS(x,y)|^2\, dx\, dy\right]^{-1} . \tag{13}$$

For tracking in elevation, xS(x,y) would be replaced with yS(x,y).

As might be expected the optimal local oscillator field distribution is the product of the distance from the center of the detector and the signal field amplitude. The distance term can be thought of as a "lever arm," where a longer lever arm implies more sensitivity to angular information. Note that for an infinitely large and infinitely fine detector array the local oscillator could be arbitrarily shaped and with the proper linear processing of each detector element output the same bound can be achieved. To simultaneously achieve both azimuth and elevation bounds would require such processing, since one local oscillator field cannot simultaneously optimally process azimuth and elevation. It is easy to show that for two dimensional tracking, an infinite area quadrant detector, and equal weighting of azimuth and elevation tracking errors L(x,y) = (x+y)S(x,y) best minimize the overall tracking error. Other suboptimal local oscillator fields will be discussed later.

---

[2] Note that the sign of the discriminator is dependent on the sign of $\Delta\omega$. If there is uncertainty in $\Delta\omega$, this must be taken into account in order to maintain tracking-loop stability.

It was previously stated that the optimal tracking performance bounds should be the same in the focal plane as the pupil plane. We will show that the respective bounds on NESD are the same. It is well known that under the paraxial propagation approximation, the field distribution in the focal plane (or far field) can be related to the field distribution in the pupil plane by a scaled two dimensional Fourier transform multiplied by a phase term [7]. Using this property as well as Parseval's theorem the above expressions can be rewritten as

$$L(x,y) = \frac{\partial S(x,y)}{\partial x} \tag{14}$$

$$NESD_{opt} = \left[\frac{\eta P_s}{h\nu} \iint_{-\infty}^{\infty} \left| \frac{\partial S(x,y)}{\partial x} \right|^2 dx\, dy \right]^{-1} \tag{15}$$

where $S(x,y)$ and $L(x,y)$ are the signal and local oscillator amplitudes in the focal plane, respectively. This bound is the same as that derived for the noise equivalent spectral density of a heterodyne spatial tracking system operating in the focal-plane [1]. Note that it is 3 dB worse than the (minimum mean-square estimation) bound for a signal shot-noise limited direct detection spatial tracking system[8]. It is not surprising that the heterodyne detection performance bounds in the focal plane and pupil plane are the same since the two field distributions are related by a linear Fourier transform. As one might expect, the two optimal processing techniques (LO shapes) are also related by a Fourier transform. The easy access to both the pupil plane and its transform the focal plane is an attractive feature of optical systems. However, these two processing techniques are analogous to amplitude comparison monopulse and phase comparison monopulse which are used in conventional radar systems [9,10].

In the pupil plane, plane wave and Gaussian field distributions can be represented by

$$S(x,y) = \sqrt{\frac{4}{\pi d^2}}\ \mathrm{circ}\left(\frac{2\sqrt{x^2+y^2}}{d}\right) \qquad \text{Plane Wave} \tag{16}$$

$$S(x,y) = \sqrt{\frac{2}{\pi \omega_s^2}}\ \exp\left[-\frac{x^2+y^2}{\omega_s^2}\right] \qquad \text{Gaussian} \tag{17}$$

where d is the diameter of the plane wave, ω_s is the 1/e amplitude of the Gaussian field, and circ(x) is 1 for $|x| < 1$ and 0 otherwise. The focal-plane amplitudes are then given by

$$S(x,y) = \sqrt{\frac{1}{4\pi}}\ \frac{\pi d}{\lambda f}\ \frac{2 J_1\left(\frac{\pi d}{\lambda f}\sqrt{x^2+y^2}\right)}{\frac{\pi d}{\lambda f}\sqrt{x^2+y^2}} \qquad \text{Airy Disc} \tag{18}$$

$$S(x,y) = \sqrt{\frac{2}{\pi\left(\frac{2f}{k\omega_s}\right)^2}}\exp\left[-\frac{x^2+y^2}{\left(\frac{2f}{k\omega_s}\right)^2}\right] \qquad \text{Gaussian} \tag{19}$$

where f is the focal length of the lens used to transform from the pupil plane to the focal plane.

To include the effect of tracking errors one either multiplies S(x,y) by $\exp[-jk(x\theta_x + y\theta_y)]$ in the pupil plane or shifts S(x,y) by $S(x - f\theta_x, y - f\theta_y)$ in the focal plane. The resulting bounds on the NESD are given by

$$NESD \geq \left[\frac{\eta P_s}{h\nu}\frac{\pi^2}{4}\frac{1}{\left(\frac{\lambda}{d}\right)^2}\right]^{-1} \qquad \text{Plane Wave or Airy Disc} \tag{20}$$

$$NESD \geq \left[\frac{\eta P_s}{h\nu}\pi^2\frac{1}{\left(\frac{\lambda}{\omega_s}\right)^2}\right]^{-1} \qquad \text{Gaussian} \tag{21}$$

3. SUBOPTIMAL LOCAL OSCILLATORS DISTRIBUTIONS

The on-axis noise-induced tracking bounds developed in the previous section, which are valid for an infinitely large and infinitely fine detector array, were shown to be independent of the detection plane. We also note that it is well known that the bound on the sum channel mode-matching efficiency is also independent of the detection plane. In this section, the detector array will be restricted to be a simple quadrant detector and the local oscillator will be restricted to one that achieves the same performance in azimuth and elevation. Although under such restrictions for a given local oscillator pattern the sum channel mode-matching efficiency is still independent of the detection plane, the tracking bounds are not.

We will investigate two suboptimal local oscillator patterns. A plane-wave signal field is assumed since it closely models the received signal for most systems. Two suboptimal local oscillators to be considered are a plane wave matched to the signal field and a truncated Gaussian field. A plane-wave local oscillator is of interest since it will maximize the power in the sum channel thus maximizing communication or radar signature performance. A truncated Gaussian field is of interest because many lasers naturally emit Gaussian fields, which cannot be precisely shaped into a plane wave without a prohibitive loss in the useable local oscillator power. For a plane-wave local oscillator field matched to the signal

$$\text{NESD} = \left[\frac{\eta P_s}{h\nu}\frac{16}{9}\frac{1}{\left(\frac{\lambda}{d}\right)^2}\right]^{-1} \qquad \text{Matched Plane Wave in Pupil Plane} \quad . \tag{22}$$

Thus for a plane-wave signal field, a local oscillator mode matched to the sum channel is within 1.4 dB of the optimal single-axis tracking performance (Equation 20).[3] It is of interest to compare this to the focal-plane case where the local oscillator is matched to the Airy disc. This was shown to be [1]

$$\text{NESD} = \left[\frac{\eta P_s}{h\nu}\frac{64}{9\pi^2}\frac{1}{\left(\frac{\lambda}{d}\right)^2}\right]^{-1} \qquad \text{Matched Airy Disc in Focal Plane} \quad . \tag{23}$$

Thus, in the focal plane a local oscillator matched to the signal field incurs over 5.3 dB of loss with respect to the single-axis tracking bound. The goal of simultaneously optimizing communication and tracking performance with a quadrant detector is more closely met in the pupil plane than in the focal plane.

[3] In this paper, a comparison in terms of dB refers to the increase in signal power that is required in order to maintain the same NESD.

In the pupil plane, if the signal is a plane wave and the local oscillator is a truncated Gaussian field, then the sum channel mode matching efficiency and the pupil plane and focal plane NESD are given by

$$|m(0)|^2 = 8\left(\frac{1-\exp\left(-\frac{1}{4}\left(\frac{d}{\omega_l}\right)^2\right)}{\left(\frac{d}{\omega_l}\right)\left[1-\exp\left(-\frac{1}{2}\left(\frac{d}{\omega_l}\right)^2\right)\right]^{1/2}}\right)^2 \tag{24}$$

$$\text{NESD} = \left[\frac{\eta P_s}{h\nu}\frac{1}{\left(\frac{\lambda}{d}\right)^2}\,32\left\{\frac{\sqrt{\pi}\,\text{erf}\left(\frac{1}{2}\left(\frac{d}{\omega_l}\right)\right) - \left(\frac{d}{\omega_l}\right)\exp\left(-\frac{1}{4}\left(\frac{d}{\omega_l}\right)^2\right)}{\left(\frac{d}{\omega_l}\right)^2\left[1-\exp\left(-\frac{1}{2}\left(\frac{d}{\omega_l}\right)^2\right)\right]^{1/2}}\right\}^2\right]^{-1} \quad \text{Pupil Plane} \tag{25}$$

$$\text{NESD} = \left[\frac{\eta P_s}{h\nu}\frac{1}{\left(\frac{\lambda}{d}\right)^2}\,8\left\{\frac{\left(\frac{d}{\omega_l}\right)\int_0^1 dt\, t\exp\left(-\frac{1}{4}\left(\frac{td}{\omega_l}\right)^2\right)\int_0^\infty dr\, J_2(r)\,J_0(tr)}{\left[1-\exp\left(-\frac{1}{2}\left(\frac{d}{\omega_l}\right)^2\right)\right]^{1/2}}\right\}^2\right]^{-1} \quad \text{Focal Plane} \tag{26}$$

where ω_l is the 1/e amplitude of the local oscillator field. These three expressions are plotted in Figure 5 relative to their optimum values.[4] In the limit as (d/ω_l) becomes small it is straightforward to show that these results agree with the matched plane wave and Airy disc results above. For $d/\omega_l \le 2.3$ the tracking performance of the pupil-plane system is superior. For $d/\omega_l \ge 2.3$ the focal-plane system is superior. This is expected since, in the pupil plane, the most sensitive angular information is near the edges of the signal field. As the local oscillator field becomes more and more Gaussian, this angular information is "amplified" by the local oscillator field less and less. Conversely, in the focal plane as the local oscillator field becomes more Gaussian, its diffraction pattern in the focal plane becomes wider. At first this wider local oscillator pattern in the focal plane increasingly weights the angular sensitive area of the signal pattern (areas of large slope) until an optimum value of $d/\omega_l = 3.1$ is reached. Beyond this value the local oscillator pattern is spread too widely and the performance suffers.

In order to maximize the mode matching efficiency in the sum channel, the desire to shape the local oscillator pattern into a plane wave is clear. Of course the power in the local oscillator field delivered to the detectors is reduced as the beam is shaped. This power loss is simple to calculate and is given by

$$\text{LO Power loss} = 1 - \exp\left(-\frac{1}{2}\left(\frac{d}{\omega_l}\right)^2\right) \quad . \tag{27}$$

This expression is also plotted in Figure 5. There is a large penalty in delivered local oscillator power for $d/\omega_l < 1$.

[4]The optimum value for m is 1 and the optimum value for both NESD values is given in Equation 20.

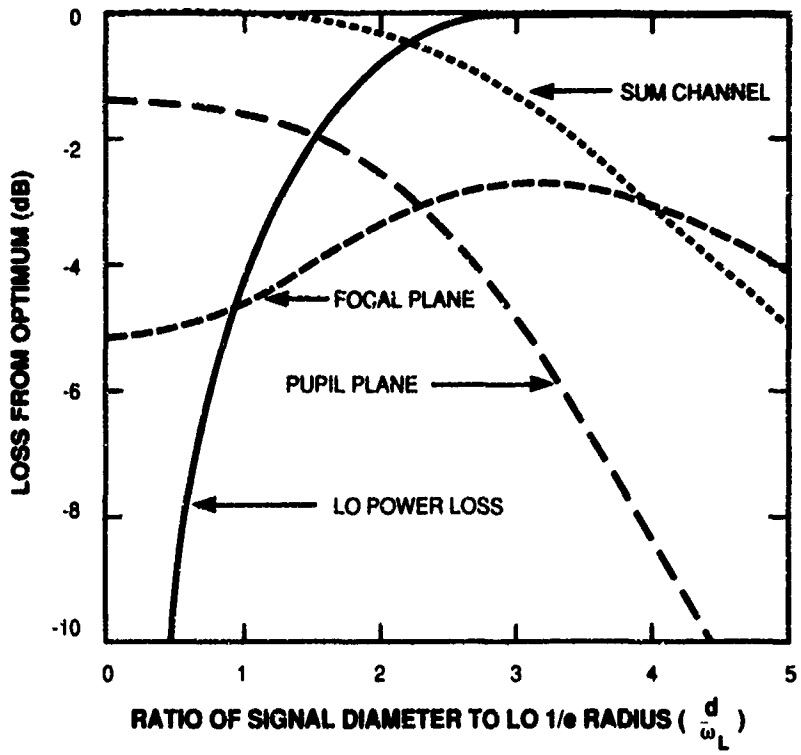

111375-6

Figure 5. Comparison of pupil plane and focal plane sum and difference channel mode-matching efficiencies and LO power loss.

As an example of the trade-off between simultaneously optimizing communication and tracking performance we refer to the Laser Intersatellite Transmission Experiment (LITE). The anticipated operating point for the LITE local oscillator field is $d/\omega_l = 2$ [Reference 11]. This value was chosen to minimize the communication channel mode matching loss (< 0.35 dB) while also minimizing the loss in local oscillator power (< 0.63 dB). The desire to minimize the communication signal power loss is obvious. The need to minimize the loss of local oscillator power stems from the desire to keep the signal levels above the thermal noise in the front-end amplifiers. At this value of d/ω_l pupil-plane processing only slightly out-performs the focal-plane system (~ 0.8 dB). The pupil-plane tracking performance is approximately 2.7 dB from optimum and the focal-plane tracking performance is approximately 3.5 dB from optimum.

So far we have only considered coherent detection followed by coherent demodulation of the I F currents. In practice, due to nonzero laser line-widths and low received signal power, coherent demodulation is not possible. For high I.F. SNR ratios the NESD expressions are still valid. However, for low I F SNR the expressions for tracking performance are worse than these equations predict [1]. The exact details of the non-coherent demodulation penalty is very dependent on the particular processing. However, for many demodulation schemes (i.e., square-law and envelope) the NESD will be proportional to the product of the difference channel mode matching efficiency and the sum channel mode matching efficiency. That is

$$\text{NESD} \sim \left[\frac{\left(\int_0^\infty \int_0^\infty \frac{\partial S(x,y)}{\partial x} L(x,y)\, dx\, dy \right)^2}{\int_0^\infty \int_0^\infty |L(x,y)|^2\, dx\, dy} \; \frac{\left(\int_0^\infty \int_0^\infty S(x,y)\, L(x,y)\, dx\, dy \right)^2}{\int_0^\infty \int_0^\infty |L(x,y)|^2\, dx\, dy} \right]^{-1} \quad \text{Focal Plane} \qquad (28)$$

$$\text{NESD} \sim \left[\frac{\left(\int_0^\infty \int_0^\infty S(x,y)\, L(x,y)\, kx\, dx\, dy \right)^2}{\int_0^\infty \int_0^\infty |L(x,y)|^2\, dx\, dy} \; \frac{\left(\int_0^\infty \int_0^\infty S(x,y)\, L(x,y)\, dx\, dy \right)^2}{\int_0^\infty \int_0^\infty |L(x,y)|^2\, dx\, dy} \right]^{-1} \quad \text{Pupil Plane} \cdot \qquad (29)$$

The local oscillator distribution (for two-axis tracking and assuming a quadrant detector) which maximizes these expressions is easily found by optimizing the linear combination of either $\{S(x,y), \partial S(x,y)/\partial x + \partial S(x,y)/\partial y\}$ for focal-plane processing or $\{S(x,y), xS(x,y) + yS(x,y)\}$ for pupil-plane processing. It was previously found that in the case of focal-plane processing, that $(0.315)^2$ bounded the quantity in square brackets[5]. For pupil-plane processing the quantity in square brackets is less than $(0.401)^2$. Thus, there is only 1.0 dB of improvement available with pupil-plane tracking performance when operating on-axis at low SNR. It was also determined that a local oscillator distribution matched to the sum channel ($(0.212)^2$) was 1.7 dB from its low SNR bound [1]. For pupil-plane processing a local oscillator distribution matched to the sum channel $[(0.333)^2]$ is within 0.80 dB from this bound.

The performance of the pupil-plane and focal-plane tracking systems operating at low I F SNR with a local oscillator that is a truncated Gaussian field in the pupil plane can be seen in Figure 5. The relative tracking performance (in dB) is given by one-half the distance between the pupil-plane and the focal-plane tracking curves. For instance, for $d/\omega_l = 0.0$ the pupil-plane tracking system is superior by 2.0 dB (this is consistent with the previous paragraph), for $d/\omega_l = 2.3$ the pupil-plane and focal-plane systems have the same performance, and for $d/\omega_l = 4.0$ the focal-plane tracking system is superior by 2.7 dB.

[5] In Reference [1] the quantity is listed as 0.283^2. The difference stems from the fact that in [1] the radial derivative was used instead of $\partial S/\partial x + \partial S/\partial y$.

4. OFF-AXIS DISCRIMINATOR GAIN

As we have seen, a quadrant detector can come very close to achieving optimal tracking performance. We now investigate some of the issues associated with off-axis discriminator gain (a major factor affecting pull-in performance) of a quadrant detector based tracking system. It is straightforward to show that the sum channel discriminators in the focal plane and the pupil plane are identical by invoking the Fourier transform relationship. However, this is not necessarily true for the difference channels. Although the slope around null of the difference channel angle discriminators may be the same in the focal plane and the pupil plane, their gain away from null is not necessarily the same. This is not to say that no local oscillator distribution, electrical processing, and detector will yield precisely the same discriminator profiles in the focal plane and pupil plane, but rather that for a quadrant detector the discriminators are not necessarily the same. To illustrate this fact, the expressions for pupil-plane and focal-plane discriminators with Gaussian signal and local oscillator distributions are given by

$$\text{Sum} = \sqrt{2P_s}\ \exp\left[-\left(\frac{k\sqrt{\theta_x^2+\theta_y^2}\ \omega_s}{\sqrt{8}}\right)^2\right]\cos(\Delta\omega t) \tag{30}$$

$$\text{Az} = \sqrt{2P_s}\ \exp\left[-\left(\frac{k\sqrt{\theta_x^2+\theta_y^2}\ \omega_s}{\sqrt{8}}\right)^2\right]\frac{2}{\sqrt{\pi}}\int_0^{\frac{k\theta_x\omega_s}{\sqrt{8}}} e^{\tau^2}\,d\tau\ \sin(\Delta\omega t) \qquad \text{Pupil Plane} \tag{31}$$

$$\text{Az} = \sqrt{2P_s}\ \exp\left[-\left(\frac{k\sqrt{\theta_x^2+\theta_y^2}\ \omega_s}{\sqrt{8}}\right)^2\right]\frac{2}{\sqrt{\pi}}\int_0^{\frac{k\theta_x\omega_s}{\sqrt{8}}} e^{-\tau^2}\,d\tau\cos(\Delta\omega t) \qquad \text{Focal Plane} \tag{32}$$

These are plotted as a function of full-width half-power beamwidths in Figure 6 (one beamwidth = $2.355/(k\omega_s) = 0.375\lambda/\omega_s$). Around boresight the discriminators have the same slope and hence the same tracking performance (this is in contrast to the previous plane-wave signal and local oscillator fields which yielded discriminator gains that were different by ~4 dB). As θ becomes large, the focal-plane discriminator falls off as $\exp[-(k\theta\omega_s/\sqrt{8})^2]$, whereas the pupil-plane discriminator falls off only as $1/(k\theta\omega_s/\sqrt{8})$. For this case, the pupil-plane tracking system has the potential of having much better pull-in performance.

We now investigate the focal-plane and pupil-plane discriminator properties for a plane-wave signal pattern and a Gaussian local oscillator pattern which has been truncated in the pupil plane. Equations for the angle discriminator profiles are given below

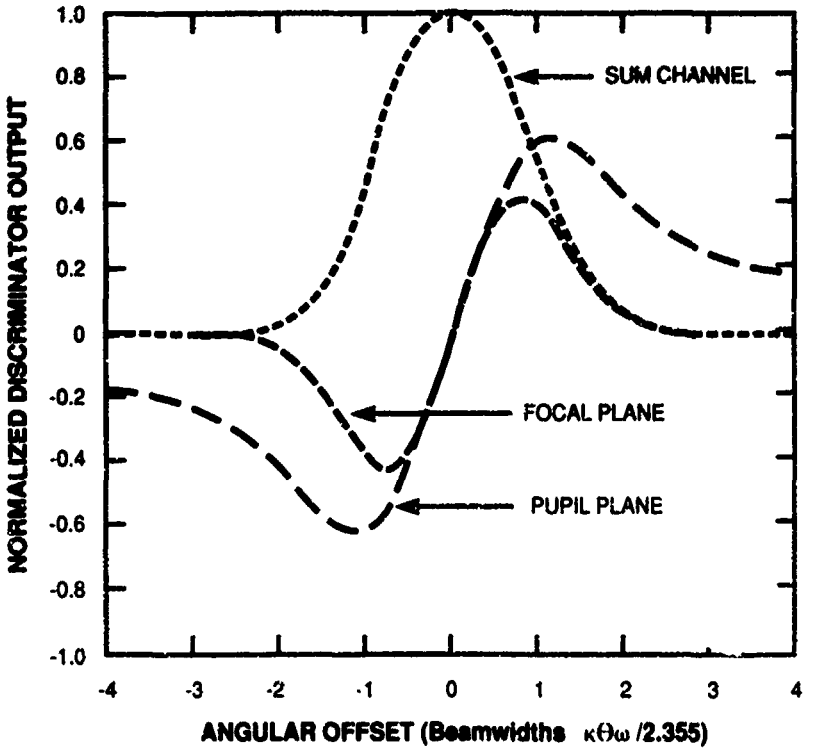

111375-7

Figure 6. Comparison of matched Gaussian focal-plane and pupil-plane discriminators.

$$\text{Sum} = \sqrt{2P_s}\,\frac{4}{\pi}c\int_0^1 dy\,\exp\left[-\frac{1}{4}\left(\frac{d\,y}{\omega_1}\right)^2\right]\cos\left(\frac{k\,d\,y\,\theta_y}{2}\right)$$
$$\int_0^{\sqrt{1-y^2}} dx\,\exp\left[-\frac{1}{4}\left(\frac{d\,x}{\omega_1}\right)^2\right]\cos\left(\frac{k\,d\,x\,\theta_x}{2}\right)\cos(\Delta\omega_t, \tag{33}$$

$$\text{Az} = \sqrt{2P_s}\,\frac{4}{\pi}c\int_0^1 dy\,\exp\left[-\frac{1}{4}\left(\frac{d\,y}{\omega_1}\right)^2\right]\cos\left(\frac{k\,d\,y\,\theta_y}{2}\right)$$
$$\int_0^{\sqrt{1-y^2}} dx\,\exp\left[-\frac{1}{4}\left(\frac{d\,x}{\omega_1}\right)^2\right]\sin\left(\frac{k\,d\,x\theta_x}{2}\right)\sin(\Delta\omega t) \qquad \text{Pupil Plane} \tag{34}$$

$$Az=\sqrt{2P_s}\,\frac{1}{\pi}c\int_{-\infty}^{\infty}dy\int_{-\infty}^{\infty}dx\ \mathrm{sgn}(x)\frac{J_1\left(\sqrt{\left(x-\pi\frac{\theta_x}{\left(\frac{\lambda}{d}\right)}\right)^2+\left(y-\pi\frac{\theta_y}{\left(\frac{\lambda}{d}\right)}\right)^2}\right)}{\sqrt{\left(x-\pi\frac{\theta_x}{\left(\frac{\lambda}{d}\right)}\right)^2+\left(y-\pi\frac{\theta_y}{\left(\frac{\lambda}{d}\right)}\right)^2}} \tag{35}$$

$$L\left(\sqrt{x^2+y^2}\right)\cos(\Delta\omega t)\qquad \text{Focal Plane}$$

$$L(r)=\int_0^1 dt\ t\exp\left[-\frac{1}{4}\left(\frac{t\,d}{\omega_1}\right)^2\right]J_0(tr) \tag{36}$$

$$c=\left\{\frac{\frac{1}{\sqrt{2}}\ \frac{d}{\omega_1}}{\left[1-\exp\left(-\frac{1}{2}\left(\frac{d}{\omega_1}\right)^2\right)\right]}\ ^{1/2}\right\} \tag{37}$$

where sgn(x) is -1 for $x < 0$ and 1 for $x > 0$. These equations are plotted as a function of the diffraction limited beamwidth (λ/d) for five different ratios of d/ω_1 (0, 0.2, 2, 4, 20) in Figures 7 to 11. The corresponding on-axis sum channel power losses are (0, 0.02, 0.34, 3.17, 17 dB), respectively. These figures are consistent with the on-axis sum and difference gains shown in Figure 5. The case where $d/\omega_1 = 0$ corresponds to matched signal and local oscillator patterns. This represents the optimal sum channel mode-matching efficiency and as was stated earlier, the gain in the linear region is ~ 4 dB larger in the pupil plane than the focal plane. Note that the gain of the difference channel away from null in the pupil plane only slightly out-performs the gain in the focal plane. There is also a large amount of ringing in the difference and sum channels as compared with the Gaussian case. The local oscillator distribution can be shaped to decrease this ringing and increase the off-axis gain at the expense of gain in the linear region and sum channel mode matching efficiency as is seen in the figures. A strong analogy exists between this effect and the trade-off of side-lobe suppression and on-axis gain that is well known in conventional antenna design [12].

These figures reinforce the earlier statement that, at both high and low I F SNR, for $d/\omega_1 < 2.3$ the pupil-plane system has superior discriminator gain, while for $d/\omega_1 > 2.3$ the focal-plane is superior. However, note that in almost all cases for large off axis angles the pupil-plane system has superior difference channel discriminator gain. Therefore, the pupil-plane systems have the potential for superior pull-in performance.

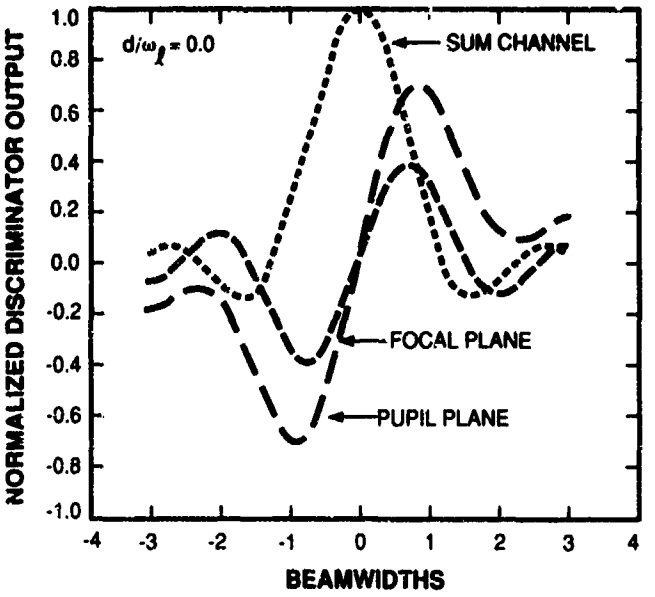

111375-8

Figure 7. Comparison of focal-plane and pupil-plane discriminators.

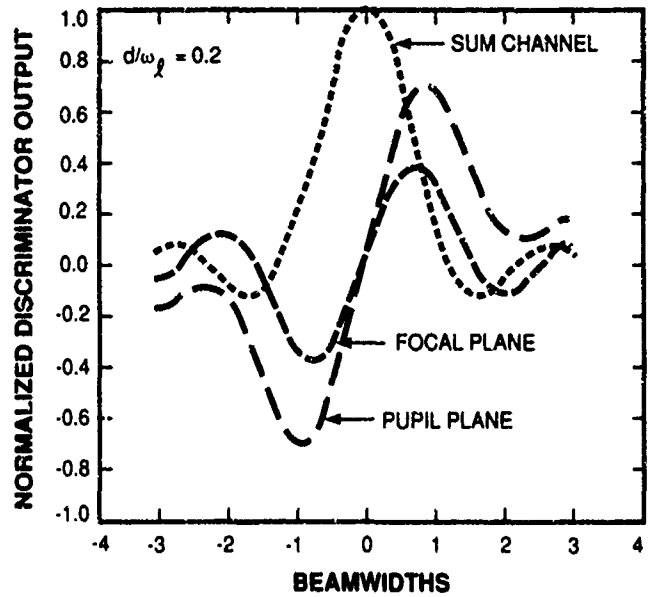

111375-9

Figure 8. Comparison of focal-plane and pupil-plane discriminators.

111375-10

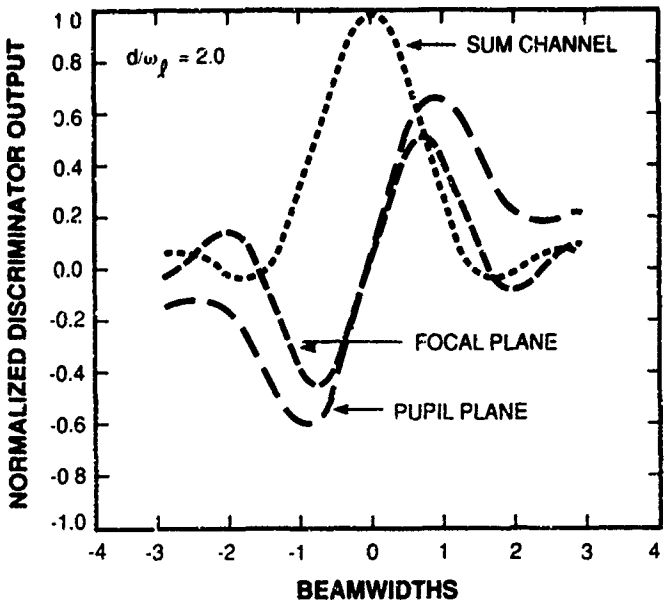

Figure 9. Comparison of focal-plane and pupil-plane discriminators.

111375-11

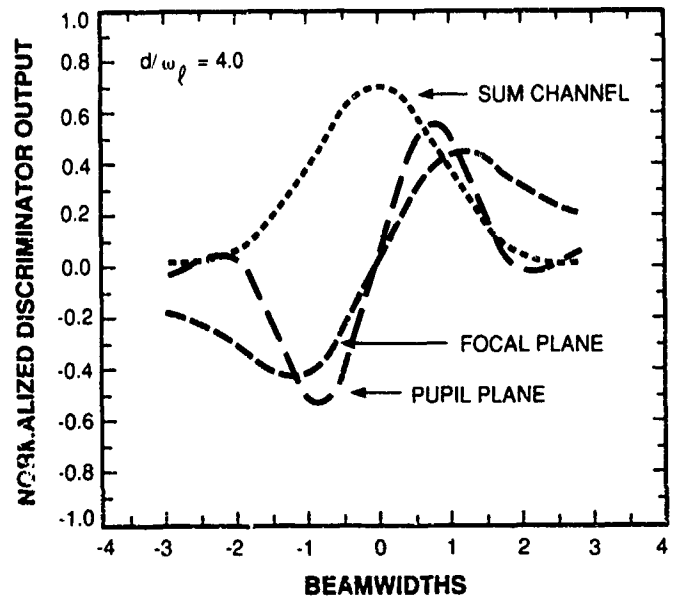

Figure 10. Comparison of focal-plane and pupil-plane discriminators.

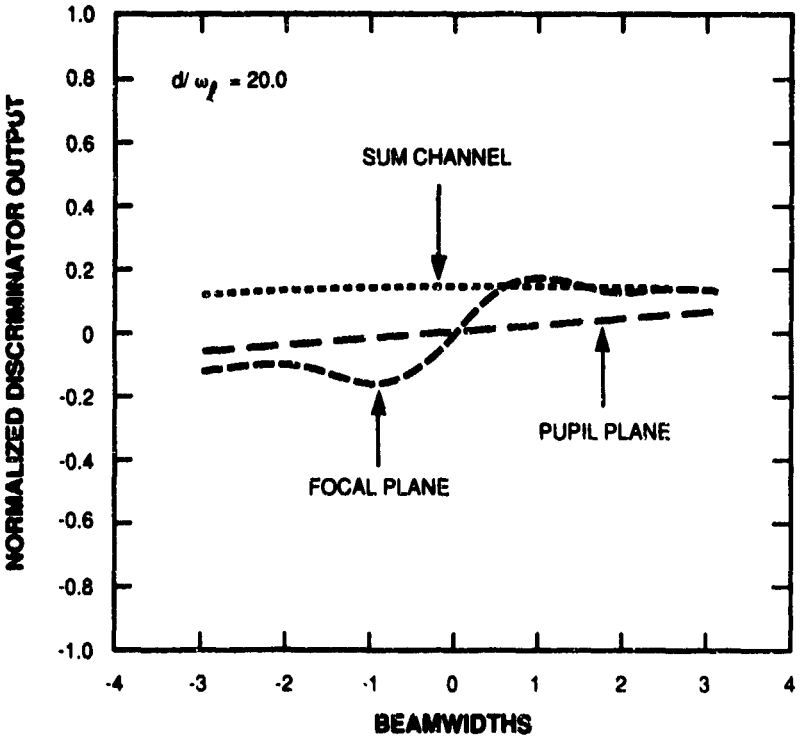

111375-12

Figure 11. Comparison of focal-plane and pupil-plane discriminators.

5. APPLICATIONS OF PUPIL-PLANE PROCESSING USING HIGHER ORDER ARRAYS

We have mainly focused on discussing results applicable to a spatial tracking system which employ a quadrant detector in the pupil plane. In this section, we briefly comment on the potential applications of using higher order detector arrays. As was stated previously, almost all of these are applicable to the focal plane; however, implementation considerations seem to favor the pupil-plane approach. Note that almost all the applications discussed have direct analogies in phased-array radars.

The use of an N × N detector array allows the receiver FOV to be electrically scanned by adding a phase gradient across the detector array outputs. This makes possible high speed scanning for acquisition as well as increased pull-in performance. The limit on the FOV is when the tilt across a detector element approaches its diffraction limited beamwidth, i.e.,

$$\theta_{max} \approx N \frac{\lambda}{d} \quad . \tag{38}$$

Beyond this point, the mode matching efficiency within each detector element decreases. Thus, for a 10 × 10 detector array the FOV can be scanned or the pull-in increased to ~10 beamwidths.

Such a detector array could also provide a point-ahead function for a lasercom link, thus eliminating the bulky point-ahead device. By boresighting the tracking detector with no phase gradient and then adding a phase gradient, a look-behind angle can be incorporated into the tracking system. The point-ahead requirement for a GEO to LEO link is ~ 40 μrad. Assuming a typical antenna beamwidth of 4 μrad, a 10 × 10 detector array would be required to fulfill the point-ahead requirement.

Atmospheric compensation could also be performed using pupil-plane processing [13]. It is well known that when communicating through the atmosphere, if the ratio of antenna diameter to transverse coherence length (d/r_o) is much larger than 1, then there is a stiff mode matching penalty (>10 dB). This penalty could be eliminated by servoing the phases of adjacent detectors in multiple detector array placed in the pupil plane provided that

$$N \approx \frac{d}{r_o} \quad . \tag{39}$$

Note that the well-known alternative of using a deformable mirror has the advantage of also compensating the transmitted beam as well as the received beam.

Other possible applications include multiple receiver apertures, adaptive antenna nulling, and lateral and longitudinal mode stabilization of laser diode arrays.

6. EXPERIMENTAL RESULTS

The optical layout and signal processing electronics are illustrated in Figures 12 and 13. Most of the experimental setup and electronics were originally designed for use in a focal-plane tracking system [14]. Consequently, the optics and electronics have not been completely optimized for a pupil-plane tracking system. However, this system demonstrates a number of key features of a single-axis, closed-loop, heterodyne spatial tracker using pupil-plane processing.

The tracker was organized as an integral part of a balanced communications receiver. Separate tracking and communication detectors are used. Throughout the discussion of the single-axis experiment, track channel references apply only to the azimuth channel. The track channel power, P_{tr}, is defined as the signal optical power in the azimuth track channel before the image splitter, or, equivalently, as the sum of the power at the right and left track detectors. The communications channel power, P_c, is defined as the sum of the signal optical power at both communications detectors. The input signal power, P_s, refers to the total signal optical power at the input to the combining beamsplitter (for lossless optics), and is equal to $P_c + P_{tr}$.

The signal beam was passed through galvonometer-driven disturbance and tracking mirrors, and then combined with the local oscillator beam on a 50:50 (s and p polarization) combining beamsplitter. The signal and local oscillator lasers were GaAlAs semiconductor diode lasers operating at a wavelength of 0.86 μm. The optical beams were each collimated Gaussian beams with 1/e radius $\omega_l = 2.65$ mm. The rms wavefront quality was interferometrically measured to be λ/33 and λ/29 (or equivalently Strehl ratios of 0.92 and 0.90) for the local oscillator and signal beams, respectively. The overlapped signal and local oscillator beams were directed to the intensity-noise-cancelling communications detectors. The sum channel mode matching efficiency was measured to be 0.85 using the technique described in [15]. The polarization beamsplitters in each of the communications paths were used to direct a portion of the received signal power to the tracking optics. In the single-axis demonstration only the azimuth tracking channel was actually used. The tracking beam was split by a knife edge, from which the light was focussed onto two tracking detectors.

The polarization of the signal and local oscillator beams at the input to the combining beamsplitter was separately adjusted (using the half-wave plates) such that equal local oscillator power was directed to all four detectors, while the signal power ratio, P_c/P_{tr}, was set to 81/19 between the communications and track paths. The signal power split represented a compromise between providing as much communications power as possible and still maintaining a sufficiently robust track signal such that adequate track performance was achieved.

Just ahead of the combining beamsplitter a quarter-wave plate was placed in the signal path, with its axes aligned with the polarization beamsplitters' axes. This introduced a 90° phase shift between the communication I F signal and each of the track channel I F signals. Such a phase shift rendered the sign of the demodulated error signal insensitive to changes in the sign of $\Delta\omega$ (see Footnote 2), the difference between the local oscillator and signal laser frequencies. In other words, the sign of the resultant discriminant was not affected by whether the local oscillator operates above or below the signal laser in

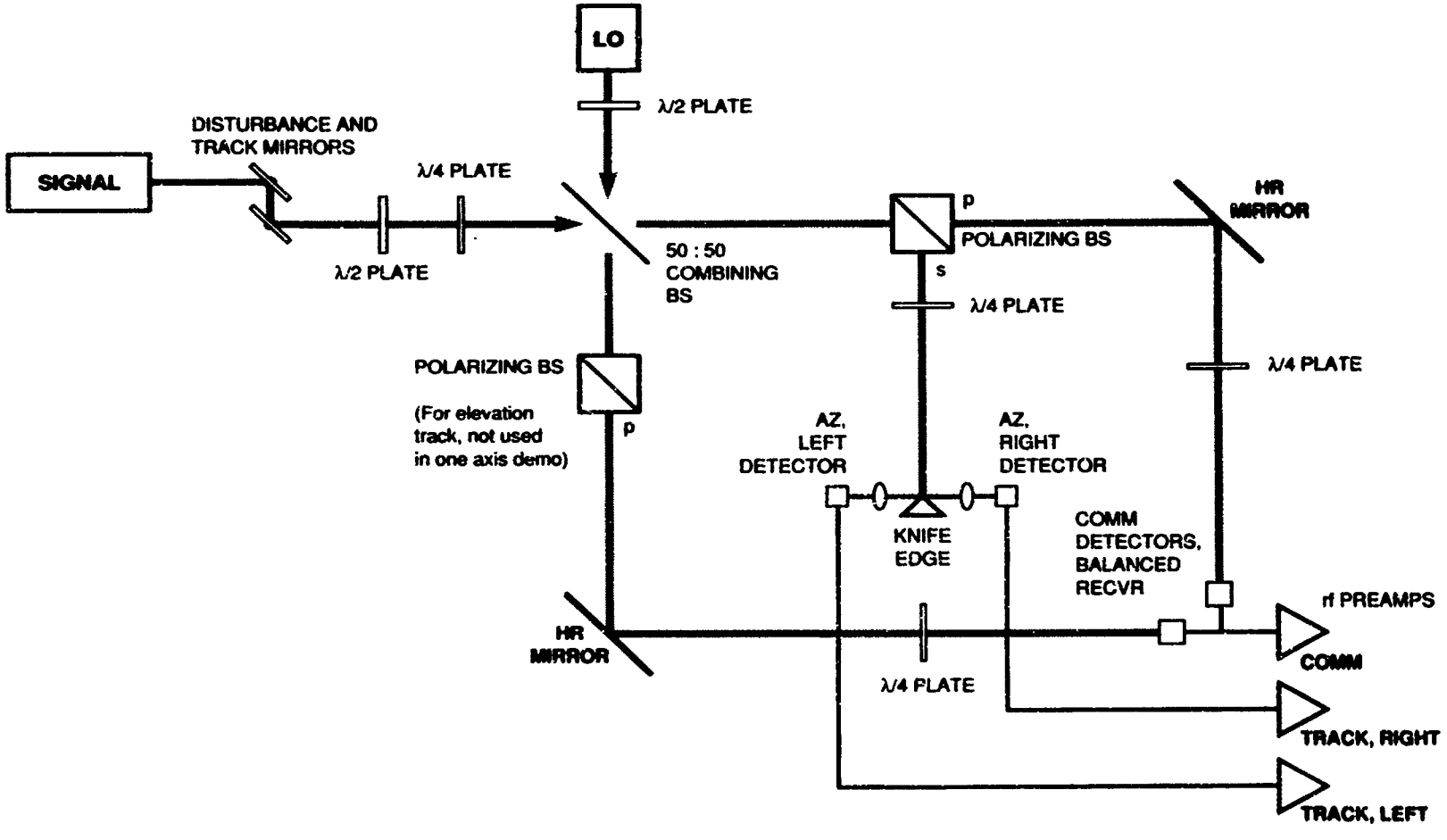

Figure 12. Optical layout, 1-axis.

111375-13

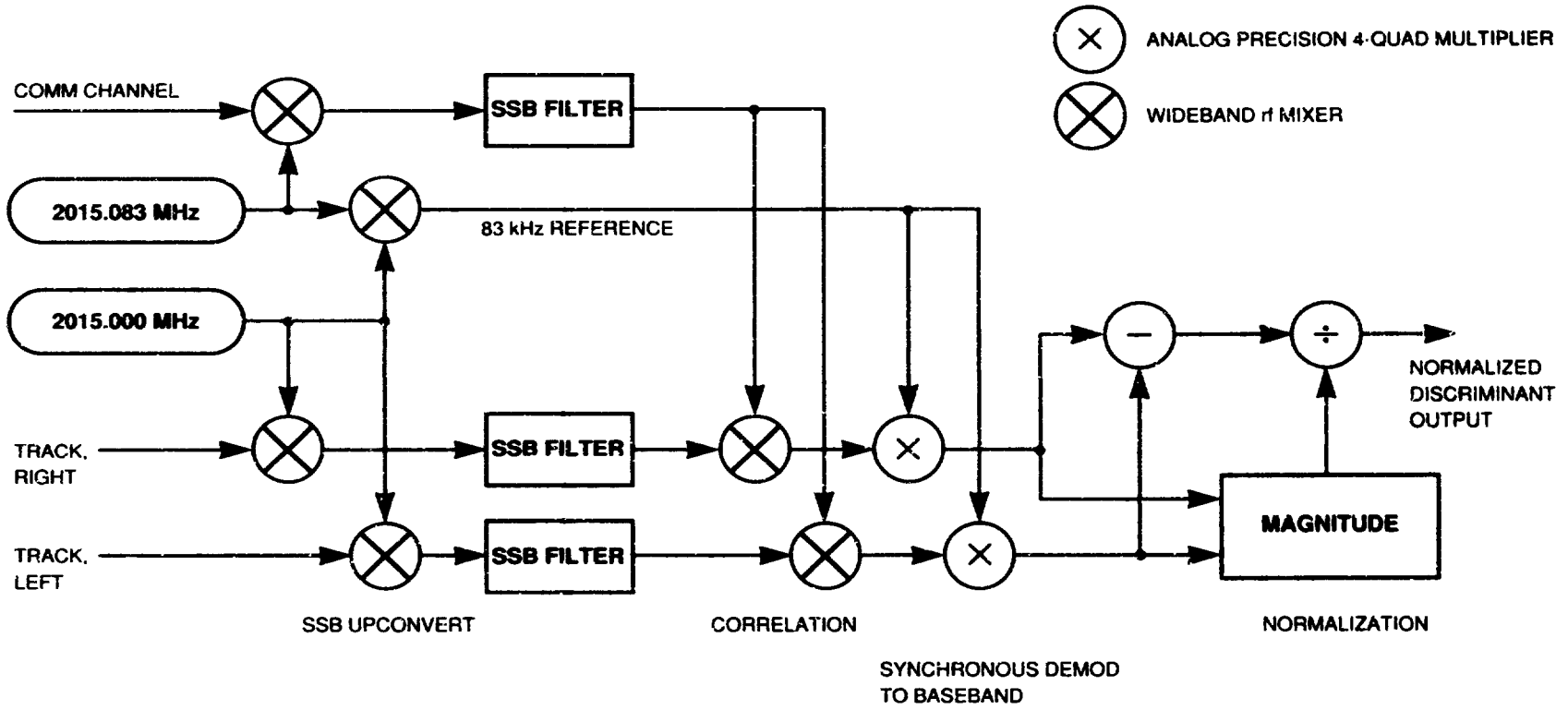

Figure 13. Correlation processing.

frequency. We note that the phase shift must be introduced optically and not electrically in order to accomplish this effect. The need to render the tracking error signal insensitive to $\Delta\omega$ may or may not be necessary in a particular system. It is dependent on frequency uncertainty during acquisition and the frequency stability during tracking.

The outputs from the tracking and communications detectors were amplified and combined as shown in Figure 13. Ideally, one would use a truly coherent processing scheme, which would yield an NEA given by (Equation 10)

$$NEA_{ideal} = \frac{1}{K_{Az}(0)} \sqrt{\frac{NEB}{\frac{\eta\gamma P_s}{h\nu}}} \tag{40}$$

where γ is included to account for the nonideal phase and amplitude distortions that give rise to a Strehl ratio less than 1. For matched Gaussian beams $K_{Az}(0) = 0.94\ BW^{-1}$. Unfortunately coherent processing is quite difficult to implement unless either the signal frequency is well known or the I F SNR is much greater than one. Because the heterodyne tracker is designed to work in a communications system which employs FSK modulation over a 500 MHz bandwidth with low received signal powers, neither of these conditions is met. Two alternatives include either square-law power detection of the heterodyne power in each side of the track channel, or the correlation technique illustrated in Figure 13.

Square-law detection suffers from excessive sensitivity to noise-induced bias at low input SNR, where the dc term due to squared broad-band noise may be 10 to 50 times the dc term due to the signal power. This dc noise term is successfully removed during subtraction of the right and left I F channel signal powers only if the right and left channels are phase and amplitude matched to better than ~ 5 % over the full input bandwidth, which is difficult.

An alternative correlation scheme employed in this experiment used the I F communications signal as a coherent reference to shift the track signals to baseband without producing a dc bias, as long as the communications and track channel noises were uncorrelated [14]. Prior to correlation the communications and track channels were offset in frequency (via SSB upconversion) by signals which differ in frequency by 83 kHz. The resultant post-correlation signals were centered at this difference frequency, instead of at baseband, in order to reduce sensitivity to the dc offsets of the wideband mixers. Subsequent synchronous demodulation shifted the error signals to baseband. Baseband processing produced an error signal normalized by the total signal power. Normalization was provided in order to maintain constant error gain, and hence constant closed-loop bandwidth, over a wide range of optical signal powers.

The correlation scheme used to generate the error discriminant is sensitive to any noise which is common to the communications and track channels. Such noise, for instance, is caused by intensity fluctuations in the local oscillator laser. Unlike the shot and amplifier thermal noises, which are uncorrelated between all of the detectors, uncancelled intensity noise can cause an offset error in the tracker which may limit performance. However, the balanced receiver [16] used in the communications channel achieved sufficient cancelling (greater than 20 dB) to make the bias due to uncancelled intensity noise a small fraction of a beamwidth.

For a shot-noise-limited system the ideal NEA for the correlation scheme can be written as

$$NEA_{ideal} = \frac{1}{K_{Az}(0)} \sqrt{\frac{NEB}{\frac{\eta\gamma P_{tr}}{h\nu}}} \left[1 + \frac{W}{\frac{\eta\gamma P_c}{h\nu}} \right]^{1/2} \tag{41}$$

where W is the noise equivalent bandwidth of the i.f. bandpass filters. The first two terms are identical to the ideal coherent demodulated NEA result given in Equation 40. The term in the square brackets can be interpreted as a noncoherent detection penalty and is almost identical to that given in [1]. Note that for high I F SNR there is no penalty for noncoherent detection.

The measured experimental results were worse that the ideal result given in Equation 41 for several reasons. First, excessive thermal noise in the detector amplifiers made it difficult to supply enough local oscillator power to the detectors to achieve the shot-noise limit. The communications channel noise was a factor of 2 above shot noise, while the track channel operated a factor of 3 above shot noise. Secondly, as noted above, the particular electronic processing used (SSB upconversion) in this experiment doubled the expected noise level ($\sqrt{2}$ increase in NEA). The resultant expected experimental NEA can be written as

$$NEA_{experiment} = \frac{\sqrt{2}}{K_{Az}(0)} \sqrt{\frac{NEB}{\frac{\eta\gamma P_{tr}}{3h\nu}}} \left[1 + \frac{W}{\frac{\eta\gamma P_c}{2h\nu}} \right]^{1/2} . \tag{42}$$

The unnormalized discriminant was measured, and is compared with the predicted discriminant in Figure 14. The predicted discriminant for the correlation based tracker is the product of the sum channel and difference channel discriminator profiles shown in Figure 6. The on-axis gain was within 2% of the theoretically predicted gain for matched Gaussian beams (Equations 30 and 31), while the off-axis behavior is also in excellent agreement with theory. The communications channel falls off in amplitude more quickly than either half of the track channel, which means that the off-axis performance of the communications-track product is dominated by the communications channel.

The rms noise over a bandwidth of 1 to 3 kHz was measured at the tracker output over a 25 dB range of input signal optical power. In order to specifically characterize the shot-noise limit of the angle sensor, the noise was measured with the feedback loop open, and at frequencies well above the acoustic and mechanical disturbances which dominated the noise spectrum below 200 Hz with the loop open. Because the shot noise spectrum was flat within the measurement region of interest (0 to 3 kHz), the shot noise contribution within a 2 kHz bandwidth was the same from 1 to 3 kHz as from 0 to 2 kHz. The NEA was obtained by dividing this rms noise by the measured discriminant gain at boresight. The resultant NEA vs input optical power for the pupil-plane tracker is plotted in Figure 15. In addition, the NEA bound using the optimum local oscillator (Equation 21) and $\eta = 1$, the ideal NEA produced via correlation, with a matched Gaussian local oscillator, $\eta = 0.73$, and $\gamma = 0.85$, and the predicted experimental NEA are plotted for comparison. We note that the measured NEA was 1.7 dB (in required input signal

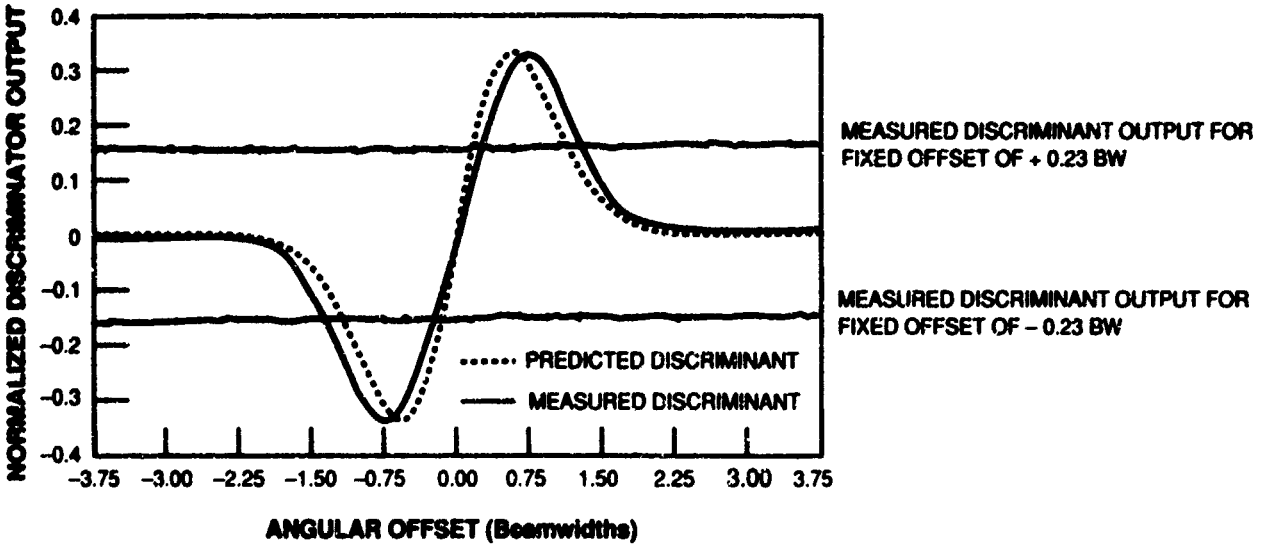

Figure 14. Pupil-plane discriminant.

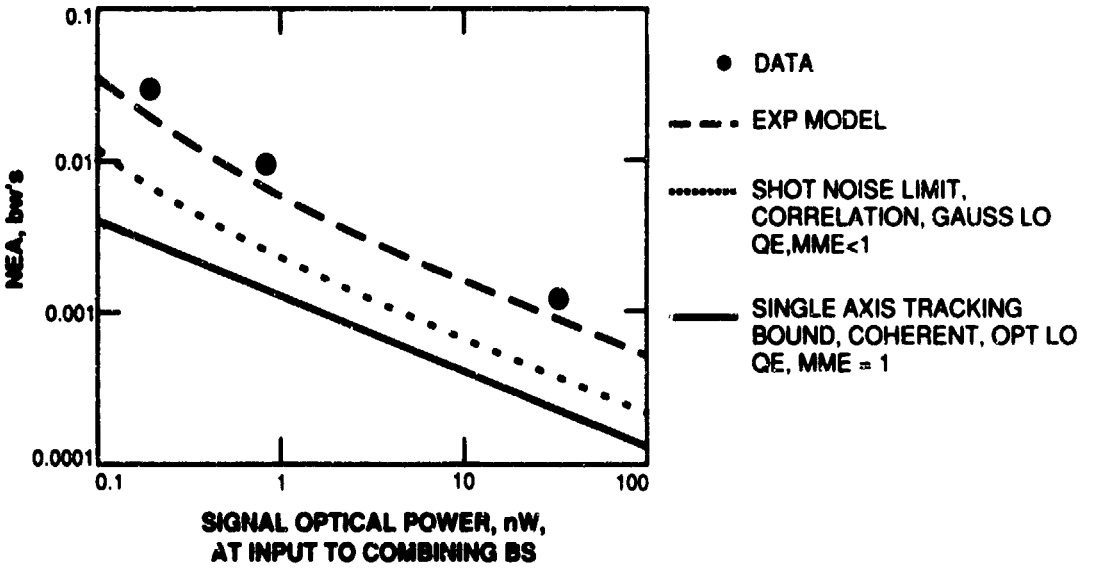

Figure 15. NEA vs signal optical power.

power) above the predicted (experimental model) NEA. Further measurements isolated this discrepancy to the communications channel SNR prior to correlation. If the measured SNR in the communication channel is used to predict the experimental NEA, excellent agreement results, which validates the analysis of the correlation process.

The -3 dB closed loop bandwidth of the tracking loop was measured at 1.3 kHz. Higher bandwidth could have been achieved but was not necessary for this application [8]. The closed loop and rejection transfer functions are shown in Figure 16. Normalization of the on-axis gain by the sum channel signal made the closed response of the tracker insensitive to input signal optical power variation over a 25 dB range.

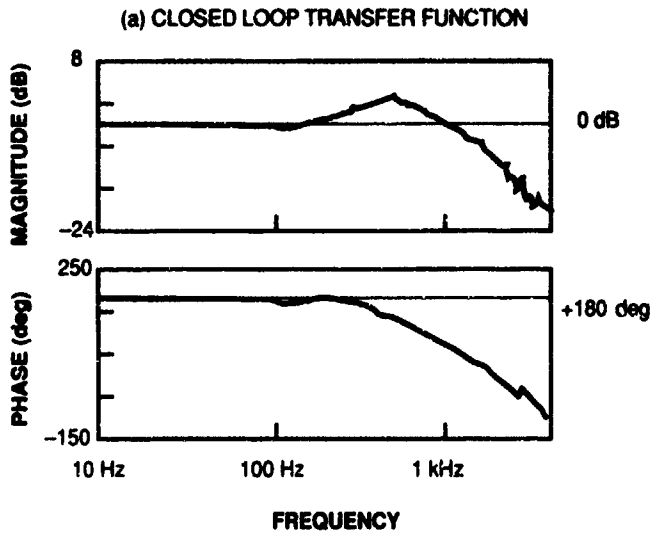

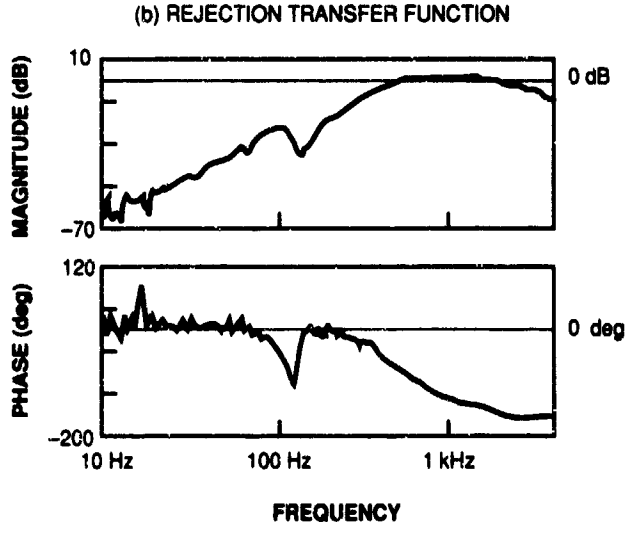

111375-17

Figure 16. Heterodyne tracker closed loop response.

7. CONCLUSION

We have shown that the theoretical tracking bounds for a spatial tracking system using coherent detection in the pupil plane is identical to the more conventional focal-plane processing technique. More important, we have shown that when implementation issues such as receiver complexity are considered, the pupil-plane system offers a number of important advantages over the focal-plane system. For instance, with a quadrant detector the optimum communication and tracking local oscillator fields are more closely matched in the pupil plane than in the focal plane. This fact leads to a potential 4 dB improvement over focal-plane processing. Also shown was an increased off-axis discriminator gain which leads to increased pull-in performance. Other implementation issues such as detector dead zone, cross talk, and alignment sensitivity were shown to be improved in the pupil-plane system.

The performance of a Gaussian local oscillator distribution truncated in the pupil plane was also investigated. It was shown that for $d/\omega_1 \leq 2.3$ the pupil-plane tracking system was superior for both high and low I F SNR. For $d/\omega_1 \geq 2.3$ the focal-plane tracking system had higher discriminator gain. However, the utility of this region is minimized by the fact that the sum channel mode matching efficiency is lower making this region an undesirable operating point.

Experimental measurements on the noise performance and dynamics of a single-axis closed-loop tracking system using detection in the pupil plane were presented. Although the system (especially the electronics) was not yet optimized for pupil plane detection, the experimental results confirm the basic concept and many of the theoretical predictions.

REFERENCES

1. E. A. Swanson and V. W. S. Chan, "Heterodyne Spatial Tracking System for Optical Space Communication," IEEE Trans. Commun., Vol. COM-34, No. 2 (February 1986), DTIC AD 172604.
2. L. J. Sullian, "Infrared Coherent Radar," SPIE, Vol. 227 (1980).
3. R. Teoste, W. J. Scouler, and D. L. Spears, "Coherent Monopulse Tracking with a 10.6 μm Radar," IEEE OSA Conf. Laser Eng. Appl., Washington, DC (June 2, 1977).
4. R. H. Kingston, "Coherent Optical Radar," Opt. News (1977).
5. J. H. McElroy *et al.*, "CO_2 Laser Communication System for Near-Earth Space Applications," IEEE Proceedings, Vol. 65, No. 2 (February 1977).
6. T. S. Wei and R. M. Gagliardi, "Direct Detection vs Heterodyne in Optical Beam Tracking," SPIE Proceedings, Vol. 739, 1987
7. J. W. Goodman, *Introduction to Fourier Optics* (McGraw Hill, New York, 1968).
8. E. A. Swanson and J. K. Roberge, "Design Considerations and Experimental Results for Direct Detection Spatial Tracking Systems," Technical Report 844, MIT Lincoln Laboratory, (April 1989).
9. M.I. Skolnick, *Radar Handbook*, Chapter 21 (McGraw Hill, New York, 1970).
10. D.K. Barton. *Radar System Analysis*, Chapter 9 (Artech, 1979).
11. R. S. Bondurant *et al.*, "Opto-Mechanical Subsystem for Space-Based Coherent Optical Communication," SPIE Proceedings, Vol. 996 (September 1988).
12. W. L. Stutzman and G. A. Thiele, *Antenna Theory and Design* (Wiley, 1981).
13. C. L. Hayes *et al.*, "Experimental Test of an Infrared Phase Conjugation Adaptive Array," J. Opt. Soc. Am.. Vol. 67, No. 3 (March 1977).
14. G. M. Carter, K. A. Winick, and D. J. Bernays, "Wideband Heterodyne Spatial Tracking for Optical Space Communication," to be published.
15. K. A. Winick and P. Kumar, "Spatial Mode Matching Efficiencies for Heterodyned GaAlAs Semiconductor Lasers," J. Lightwave Tech., LT-6, 513 (1988).
16. G. L. Abbas, V. W. S. Chan, and T. K. Yee, "Local-Oscillator Excess-Noise Suppression for Homodyne and Heterodyne Detection," Opt. Lett., Vol. 8, No. 8 (August 1983).

UNCLASSIFIED

SECURITY CLASSIFICATION OF THIS PAGE

REPORT DOCUMENTATION PAGE

1a. REPORT SECURITY CLASSIFICATION Unclassified	1b. RESTRICTIVE MARKINGS
2a. SECURITY CLASSIFICATION AUTHORITY	3. DISTRIBUTION/AVAILABILITY OF REPORT Approved for public release; distribution is unlimited.
2b. DECLASSIFICATION/DOWNGRADING SCHEDULE	
4. PERFORMING ORGANIZATION REPORT NUMBER(S) Technical Report 823	5. MONITORING ORGANIZATION REPORT NUMBER(S) ESD-TR-88-312
6a. NAME OF PERFORMING ORGANIZATION Lincoln Laboratory, MIT 6b. OFFICE SYMBOL *(If applicable)*	7a. NAME OF MONITORING ORGANIZATION Electronic Systems Division
6c. ADDRESS *(City, State, and Zip Code)* P.O. Box 73 Lexington, MA 02173-0073	7b. ADDRESS *(City, State, and Zip Code)* Hanscom AFB, MA 01731
8a. NAME OF FUNDING/SPONSORING ORGANIZATION HQ AF Systems Command 8b. OFFICE SYMBOL *(If applicable)* AFSC/XTKT	9. PROCUREMENT INSTRUMENT IDENTIFICATION NUMBER F19628-85-C-0002
8c. ADDRESS *(City, State, and Zip Code)* Andrews AFB Washington, DC 20334-5000	10. SOURCE OF FUNDING NUMBERS PROGRAM ELEMENT NO. 63789F; PROJECT NO. 270; TASK NO.; WORK UNIT ACCESSION NO.

11. TITLE *(Include Security Classification)*
Optical Spatial Tracking Using Coherent Detection in the Pupil Plane

12. PERSONAL AUTHOR(S)
Eric A. Swanson, Gary M. Carter, D. Jonathan Bernays, and David M. Hodsdon

13a. TYPE OF REPORT	13b. TIME COVERED	14. DATE OF REPORT *(Year, Month, Day)*	15. PAGE COUNT
Technical Report	FROM _____ TO _____	19 May 1989	46

16. SUPPLEMENTARY NOTATION
None

17. COSATI CODES			18. SUBJECT TERMS *(Continue on reverse if necessary and identify by block number)*
FIELD	GROUP	SUB-GROUP	pupil-plane processing; spatial tracking system; focal-plane processing

19. ABSTRACT *(Continue on reverse if necessary and identify by block number)*

Design considerations for a heterodyne spatial tracking system utilizing pupil-plane processing techniques and its advantages over traditional focal-plane processing are described. Noise performance bounds, optimal and suboptimal local oscillator distributions, pull-in performance, and applications other than spatial tracking are discussed. Experimental verification of a one-axis closed-loop tracking system is presented.

20. DISTRIBUTION/AVAILABILITY OF ABSTRACT ☐ UNCLASSIFIED/UNLIMITED ☒ SAME AS RPT. ☐ DTIC USERS	21 ABSTRACT SECURITY CLASSIFICATION Unclassified
22a NAME OF RESPONSIBLE INDIVIDUAL Lt. Col. Hugh L. Southall, USAF	22b. TELEPHONE *(Include Area Code)* (617) 981-2330 22c. OFFICE SYMBOL ESD/TML